

Malware-on-the-Brain: Illuminating Malware Byte Codes with Images for Malware Classification

Fangtian Zhong, Zekai Chen, Minghui Xu, Guoming Zhang, Dongxiao Yu, Xiuzhen Cheng, *Fellow, IEEE*

Abstract—Malware is a piece of software that was written with the intent of doing harm to data, devices, or people. Since a number of new malware variants can be generated by reusing codes, malware attacks can be easily launched and thus become common in recent years, incurring huge losses in businesses, governments, financial institutes, health providers, etc. To defeat these attacks, malware classification is employed, which plays an essential role in anti-virus products. However, existing works that employ either static analysis or dynamic analysis have major weaknesses in complicated reverse engineering and time-consuming tasks. In this paper, we propose a visualized malware classification framework called VisMal, which provides highly efficient categorization with acceptable accuracy. VisMal converts malware samples into images and then applies a contrast-limited adaptive histogram equalization algorithm to enhance the similarity between malware image regions in the same family. We provided a proof-of-concept implementation and carried out an extensive evaluation to verify the performance of our framework. The evaluation results indicate that VisMal can classify a malware sample within 4.0 ms and have an average accuracy of 96.0%. Moreover, VisMal provides security engineers with a simple visualization approach to further validate its performance.

Index Terms—Classification; Histogram Equalization; Malware; Visualization.



1 INTRODUCTION

MALWARE classification refers to the process of grouping malware samples with similar features to effectively classify unknown malware. Features can be categorized as either static or dynamic, with the former being extracted based on a byte-code sequence, binary assembly instructions, or an imported Dynamic Link Library (DLL), and the latter on runtime file system activities, terminal commands, network communications, and function or system call sequences. Since malware samples in the same family normally have similar static or dynamic features, which could be extracted via machine learning algorithms, security vendors and researchers usually utilize them as useful clues for effective malware classification [1], [2].

However, malware feature extraction, whether static or dynamic, is a non-trivial task. The extraction of static features requires security professionals to have a good command of the structure of malware binaries. For instance, to extract an imported Dynamic Link Library in a Windows program, developers have to know the PE before parsing two structures in the order of DataDirectories followed by Import or Import Address Table [3]. Additionally, it is even worse when encryption or compression is applied to malware binaries as reverse analysis is needed [4]. On the other hand, although the extraction of dynamic features obviates the conundrums and limitations of static feature

extraction, dynamic analysis can only collect the behaviors of specific execution paths since it is hardly possible to traverse all of them. Meanwhile, dynamic analysis is time-consuming. For instance, some applications may have multiple event handlers that should be examined for dynamic feature extraction. Nevertheless, it can be insufficient to call just the one that contains a particular API invocation; instead, multiple event handlers may need to be triggered as a “chain” in a particular order with specific inputs [5].

One can see from the above analysis that malware classification involves either very high knowledge barriers for security professionals or huge computing burdens for computers. To overcome the knowledge obstacles and improve malware classification efficiency, we have to address the following three critical challenges when designing malware classification schemes. First, since the ultimate purpose of malware classification is to precisely classify different malware samples, the extracted features should uniquely represent the samples and maintain the similarity for malware in the same family. Second, as the schemes are expected to be efficient, the time for extracting features and classifying malware samples should be limited to some degree that users can withstand. Third, even though security engineers may not have enough background knowledge about malware samples, the schemes should be easy to use and comprehend. Based on these considerations, we present a novel but simple visualized classification framework named VisMal in this paper, which aims at understanding the inner workings of malware families and disclosing the encoding art in the byte codes of malware binaries. VisMal consists of three major components: Converter, Feature Engineer, and Classifier. Converter takes charge of converting a malware sample into a 2-Dimensional grayscale image; Feature Engineer enhances the recognition of malware via strengthening the local contrast in the malware image regions and resizes

- Fangtian Zhong and Zekai Chen are with the Department of Computer Science, The George Washington University, Washington DC, USA. Emails: {squareky_zhong,zech_chan}@gwu.edu

Minghui Xu, Guoming Zhang, Dongxiao Yu and Xiuzhen Cheng (Corresponding Author) are with the School of Computer Science and Technology, Shandong University, Qingdao, 266237, China. Emails: {mhxu,guomingzhang,dxyu,xzcheng}@sdu.edu.cn

the image to a smaller one to expedite the classification process; and Classifier is used to partition malware samples into their corresponding families.

VisMal endeavors to greatly reduce the burdens on security engineers and the computing expenses on computers. Since existing works adopt either static or dynamic analysis approaches, which inevitably have drawbacks as mentioned above, it is necessary to turn our mind to pursue the essence of the malware families themselves. Note that many variants of malware samples are generated by reusing core codes [6]–[9], one can use the similarity of instruction sequences to classify different types of malware samples. We provide an implementation of VisMal and conduct extensive experimental studies to evaluate its effectiveness in terms of accuracy, efficiency, and visualization. This study makes every effort to understand malware families and discover the underlying encoding art in byte codes. Our multi-fold contributions can be summarized as follows.

- 1) We propose VisMal, a visualized malware classification framework, to efficiently distinguish different types of malware samples while in the mean time maintaining high accuracy.
- 2) By improving local contrasts of the regions in converted images, we enlarge the discernity of malware samples, which elevates the accuracy from grayscale images without extra operations.
- 3) When malware samples are compressed or encrypted, VisMal still demonstrates good performance on distinguishing different malware families.
- 4) VisMal provides a visual technique for security engineers without much knowledge about malware samples to readily validate the classification performance.

The rest of the paper is organized as follows. Section 2 introduces the most related work. Section 3 details the workflow and implementation of VisMal. Section 4 evaluates the performance of VisMal, and Section 5 concludes the paper with a discussion on future research.

2 RELATED WORK

In this section, we provide an overview on popular existing malware classification methods, considering whether they are static analysis based or dynamic analysis based.

2.1 Malware Classification Based on Static Analysis

Since static features can be directly obtained from malware files without execution but they still possess certain discernibility, many approaches based on these features were proposed to classify different malware families, which are summarized as follows.

Machine Learning-Based Approaches. Jiang *et al.* developed a K Nearest Neighbour based (KNN) model for malware classification by taking an input vector carrying codes' semantic information that comes from sensitive opcode sequences [10]. Each sensitive opcode sequence is constructed by opcodes, application programming interfaces, STR instructions, and actions. All sensitive opcode sequences are sent to Doc2vec for the generation of sensitive semantic information, and the information is then

used for classification in a pretrained KNN model. Fasano *et al.* proposed a cascade learning method to distinguish different malware families by combining a KStar classifier for the discrimination of benignware and malware with a RandomForest classifier for the identification of different malware families [11]. The cascade learner makes use of totally 12 static values as features that are calculated from each malware, including cyclomatic complexity, weighted methods per class, bad smell method calls, wakelocks with no timeout, number of location listeners, number of GPS users, etc. Blanc *et al.* trained a random forest classifier by leveraging the architectural and external attributes of malicious apps to identify different android malware families [12]. To construct these attributes for a piece of malware, an app is initially decompiled with Apktool and converted into human-readable Smali codes. These codes are then parsed by a code quality tool and finally used for the extraction of 10 attributes (e.g., XML Parsers and Network Timeouts).

DNN-Based Approaches. Jung *et al.* proposed a convolutional neural network model based on byte information to classify malware samples [13]. The extraction of byte information includes 3 steps: a malware binary file is first input to a disassembler, which returns the disassembled malware file; then byte length sequences are extracted from the disassembled malware file and used as parameters to a specific hash function; finally all hash values generated from the second step are used to construct a hash map, which is referred to as the byte information. Saxe *et al.* presented a deep feed forward neural network trained on various features extracted by static analysis for binary malware classification [14]. The features include system library import functions, ASCII printable strings, PE metadata fields in the executable, as well as byte sequences from the raw codes. They are concatenated to form a 1024-dimensional feature vector, which is fed into a four-layer feed forward network for training and further classification. Davis *et al.* developed an approach that employs a convolutional neural network to identify malware [15]. The raw disassembled codes of malware are processed to generate a vector of fixed-length features. This approach extracts the individual x86 processor instructions with diverse lengths and then apply padding or truncation to create fixed length features. The disassembled codes are also parsed to extract system library import functions to further extend the feature vector size.

Other Approaches. Kinable *et al.* investigated malware classification based on call graph clustering [16]. Each malware can be represented as multiple call graphs that consist of local functions and system library functions as vertexes and caller-callee relationships as edges. Malware programs in the same family should have minimized number of mismatches in their graphs. To compute malware mismatches, they adopted the graph edit distance that is the minimum number of elementary operations required to transform one graph to another. Mirzaei *et al.* proposed a characterization approach for malware families based on common ensembles of sensitive API calls [17]. The overall architecture of the proposed system goes through five steps: it first computes fuzzy hash values of all functions extracted from the apps in the same family; then it creates call graphs and uses the fuzzy hash values to replace the nodes (functions); next, it merges the hashed call graphs and

all edges to form an aggregated graph and assigns a unique weight to each edge; following that it inspects the results from the frequency of similar methods and the frequency of the methods' invocations in the similar methods within a family, which are used to create feature vectors at last for classification. Zhang *et al.* implemented a prototype system named DroidSIFT, a novel semantic-based approach to classify Android malware via dependency graphs [18]. They generated dependency graphs by discovering entry points and analyzing call graphs. Following the generation of dependency graphs, they leveraged both forward and backward dataflow analysis to explore API dependencies and uncover constant parameters. DroidSIFT hence uses dependency graphs to build graph databases and classifies a malware sample by producing graph-based feature vectors and then performing graph similarity queries.

2.2 Malware Classification Based on Dynamic Analysis

In contrast to static analysis, which derives properties from a program's text, dynamic analysis obtains properties by examining a running program. Approaches based on dynamic analysis are important complements to improve detective capability when static features are hard to extract due to obfuscations. In this subsection, we summarize major malware classification works based on dynamic analysis.

Machine Learning Based Approaches. Sethi *et al.* developed a machine learning based malware analysis framework for classification [19]. All malware samples are executed and analyzed on top of the Cuckoo Sandbox, which examines their run-time behaviors and returns behavioral reports that memorize their activities. The reports are further processed by a feature extraction and selection module before sent to machine learning models such as Decision Tree and Random Forest for final classification. In [20], Martin *et al.* implemented a tool termed CANDYMAN to classify Android malware by combining dynamic analysis and Markov chains. In their experiment, DroidBox was employed as the dynamic analysis tool to generate a state sequence representation for each malware. The state sequence representation is then used to model the transition probabilities between consecutive states. Once all transition probabilities are computed, they are input to a collection of machine learning algorithms (i.e., SMOTE, Random Over Sampler, Random Under Sampler, etc.) for further classification. Anderson *et al.* designed a malware classification algorithm based on graphs constructed from dynamically collected instruction traces of target executables under the Ether system [21]. Each instruction is denoted as a vertex in a graph, an edge between two nodes represents the transition from one instruction to another, and the transition probabilities are estimated by all collected traces. One can acquire a similarity matrix with each entry describing the similarity between an executable and a malware class, which is obtained by employing graph kernels, and then send the matrix to a support vector machine for classification.

DNN-Based Approaches. Dahl *et al.* trained a neural network with three hidden layers by feeding it with system API calls as well as null terminated strings extracted from the process memory [22]. A random projection technique

was used to reduce the features' dimensionality to the degree that is manageable by the neural network. Tobiyama *et al.* developed a recurrent neural network (RNN) to extract features from a detailed representation of malware process behaviors and used a convolutional neural network (CNN) to classify the outputs from the RNN [23]. Each API call represents an operation of the process, multiple API calls represent an activity, and multiple activities represent a behavior of the process. In each operation, critical information such as process name, ID, event name, and path of current directory is recorded. Zhang *et al.* proposed a low-cost feature extraction approach and an effective deep neural network architecture for accurate and fast malware classification [24]. They executed PE files inside virtual machines and used API hooks to monitor the API call traces. They also utilized a feature hashing trick to encode the API call arguments associated with the API name for each API call. The deep neural network architecture applies multiple Gated-CNNs to transform the encoding into particular feature representations that are further processed by bidirectional LSTM (long-short term memory networks) to learn the sequential correlations among API calls.

Other Approaches. Vij *et al.* proposed a novel graph signature based malware classification mechanism [25]. The graph signature uses sensitive application programming interfaces to capture the control flow that builds a bridge between sensitive APIs and the respective incidents. A dataset of graph signatures for well-known malware families is then created. A new application's graph signature is compared with the signatures in the dataset, and the application is classified into the corresponding malware family. Park *et al.* developed a malware classification algorithm called FACT via finding the maximum common subgraphs in directed function call graphs [26]. Each graph is constructed by capturing the uses of the system functions along with the parameter values when the malware program is executed in a sandboxed environment. Since malware programs belonging to the same family generally share similar behaviors by calling certain system functions, i.e., file system modification, new process spawning, network connectivity checking, registry modification, etc., their subgraphs tend to be similar to some extent. Hsiao *et al.* proposed an analysis scheme to group Android malware based on their dynamic behaviors, and to identify the behaviors of a malware family. They also applied phylogenetic tree, significant principal components, and dot matrix on different malware families to demonstrate their behavioral correlations. The proposed methods can automatically discover similar behaviors of different malware groups, extract the characteristics of each malware group, and provide security experts with the visualized information based on runtime behaviors [27].

2.3 Summary

In this paper, we present VisMal, which converts malware binaries into 2-Dimensional grayscale images and utilizes a contrast-limited adaptive histogram equalization algorithm to expand the difference in all image regions such that it is easier for our classifier to capture the similarity of malware samples in the same family. Previous works such as [1], [2], [5], [11] perform less effective when reverse

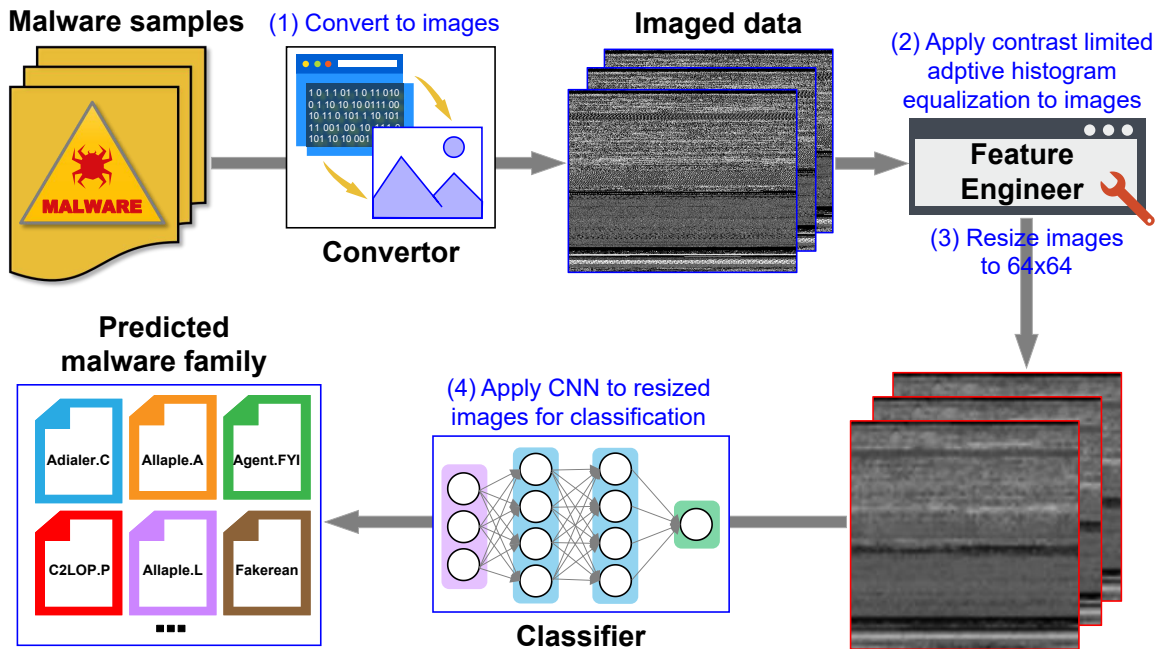


Fig. 1: Overview of the VisMal Framework

analysis is an obstacle and time is a constrained factor. VisMal cleverly bypasses the obstacles of reverse analysis by making effort to understand the properties of malware families, and discover the underlying similarity in byte codes. Additionally, VisMal processes a malware program as an image, significantly reducing the waiting time for analysis. These two features make VisMal more practical and efficient. VisMal is also different from the works such as [28]–[31] that process malware as images, which focus on statistical features of the converted image – VisMal pays attention to the understanding of the correspondence between byte codes and pixels. Besides, VisMal does not need to intentionally pick out particular statistical features for classification.

From the previous analysis, one can see that malware classification based on static features distinguishes different malware samples mainly by grouping their text and statistical information extracted from malware files. Text information includes opcode sequences, system library import functions, and ASCII printable strings, while statistical information calculated by various tools involves cyclomatic complexity, number of GPS users, and network timeouts, etc. Different from static analysis based methods, VisMal does not require the disassembling of the malware samples and the help of any tool. On the other hand, malware classification based on dynamic features deals with the running programs on top of virtual machines and examines malware samples by their programs' activities, instruction traces, API call traces, control flows, etc. In contrast to such methods, VisMal does not need to execute programs and check each execution trace to assure the reliability of classification. Besides, the selection of a distinct collection of features to uniquely represent a malware sample is not required by VisMal.

3 THE PROPOSED VISMAL FRAMEWORK

3.1 Overview of VisMal

The three-fold objectives of VisMal include: i) efficiently classify malware samples into their respective families, ii) reduce security engineers' burdens by providing automatic classification tools, and iii) offer an image-based validation method for identifying the effectiveness of classification. The framework of VisMal is presented in Fig. 1. One can see that VisMal consists of 3 components: *Converter*, *Feature Engineer*, and *Classifier*. Converter converts a malware binary into an image. Feature Engineer processes the image by a contrast-limited adaptive histogram equalization algorithm to increase the local contrast in different image regions and then resize the processed image to a smaller fixed-size one that can accelerate the process of classification. Classifier employs a shallow convolutional neural network-based model. It enables parameter sharing, a technique that applies the same small filter to all elements of the input and captures the correlation of different elements, to allow CNN to efficiently extract the local features in an image.

The workflow of VisMal is described as follows. All malware samples, whether in the training dataset or in the test datasets, need to be converted to a grayscale image according to the following procedure: a malware example is first sent to Converter for numeric conversion, which outputs an array consisting of numbers with scope between 0 and 255; then the array is reshaped according to its file size (see Table 1); following the reshaping is the feature editing and resizing processes by Feature Engineer. The output of Feature Engineer is an image array scaled to 64x64. Then it is concatenated with the corresponding malware family label. The data is randomly divided into a training dataset and test dataset by StratifiedKFold. This is a variation of KFold that returns stratified folds made by preserving the percentage

of samples for each class [32]. The training dataset is used to train Classifier. Once the classifier is well trained, one can use it to characterize the malware samples in the test dataset.

TABLE 1: Correspondence between the file size of a malware sample and the converted image width

File Size	Width	Height
$\leq 10\text{KB}$	32	(0, 312]
10KB-30KB	64	(156, 468]
30KB-60KB	128	(234, 468]
60KB-100KB	256	(234, 390]
100KB-200KB	384	(260, 520]
200KB-500KB	512	(390, 976]
500KB-1000KB	768	(651, 1302]
1000KB \leq	1024	(976, ∞)

3.2 The Components of the VisMal Framework

In this section, we detail the implementations of the three components of VisMal, namely *Converter*, *Feature Engineer*, and *Classifier*.

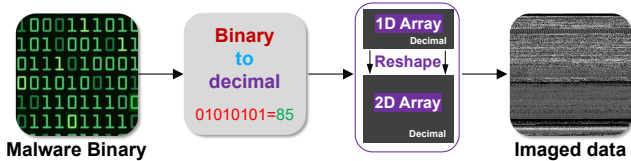


Fig. 2: Converter

3.2.1 Converter

Fig. 2 demonstrates the procedure of numeric conversion by Converter for a malware example. To convert a malware binary into a grayscale image, Converter sequentially reads the binary data in bytes, converts each byte into a decimal number ranging in [0-255] [28], then saves the number in a one-dimensional array. For instance, '0110000' is converted to 96. Every number in the array corresponds to a pixel in a grayscale image. As the resolution of a grayscale image has width and height dimensions but different malware samples vary in their file sizes, one should consider such a situation to accept diverse options of width and height. In this paper, we take a simple approach to reshape the image data (array) by following the recommended fixed-width with a variable height according to its file size, which is correspondingly transformed into a 2-Dimensional grayscale image conforming to portable network graphics (.png extension) via a built-in function, i.e., `imwrite` or `imsave`, in `cv2` library or `PIL` library. The recommended fixed image widths for distinct malware file sizes are given in Table 1 [29].

3.2.2 Feature Engineer

As suggested in [6]–[9], many variants of malware samples are generated by reusing core codes. Therefore one can use the similarity of instruction sequences to classify different malware samples. Since an instruction typically has multiple bytes and each byte corresponds to one pixel, the instruction is converted into several pixels by Converter. Thus locating

similar instruction sequences from different malware samples is equivalent to identifying regions with similar pixel values in their corresponding images. Nevertheless, similar instruction sequences from different malware samples belonging to the same malware family may exist at different positions of their files. To overcome this challenge, we resort to the image contrast to identify similar pixel regions – image regions produced by similar instruction sequences should have similar contrast values. To further improve the accuracy of Classifier, the capture of similar pixel values in different malware images should be promoted. Since the usable data of an image is normally represented by close contrast pixel values [33], increasing the contrast of an image benefits classification. Therefore, Feature Engineer adjusts pixel intensities in each image region to enhance the contrast for a malware image by applying a contrast-limited adaptive histogram equalization algorithm. This algorithm maps the narrow range of input pixel values for an image region to the whole range of the pixel values for an image, i.e., 0-255. Through this adjustment, the intensities can be better distributed on the histogram¹ for each image region by effectively spreading out the most frequent intensity values, which allows for areas of lower contrast to gain higher contrast and improves the contrast for the entire image. High contrast enhances the possibility of Classifier to identify similar pixel values in images.

Figuratively speaking, contrast-limited adaptive histogram equalization seems to be equivalent to signal transform that happens in biological neural networks so as to maximize the output firing rate of a neuron which is a function of the input statistics. The equalization algorithm contains 4 phases: Division, Cumulation, Clipping, and Transformation. Division divides an image into $a \times b$ small regions where a and b are respectively the numbers of pieces split up for the width and height of the image. A cumulation is a cumulative frequency distribution function for an image region, whose computation is shown in (1):

$$cdf(i) = \sum_{j=0}^i n_j, 0 \leq i < L \quad (1)$$

where L is the total number of gray levels (typically 256), and n_j is the number of times the pixel value j appears in an image region. Note that n_j is also called the frequency of j . As shown in Fig. 3, if the frequency of a pixel value is above the threshold `clipLimit`, Clipping is applied to assign a random value in $[0, 255]$ to some of such pixels such that no pixel can have a frequency higher than `clipLimit` (see Fig. 3); correspondingly, the histogram is adjusted to a new frequency distribution for the image region. Transformation transforms the input pixel values into output pixel values by adopting different transformation methods according to their positions in the malware image.

We use Fig. 4 as an example to illustrate the Transformation phase. In Fig. 4, the image is partitioned into 4×3 equal-sized rectangular regions. The center of each region is represented by a black dot, and each boundary region is partitioned into 4 smaller rectangles by the center lines, resulting in areas with three different colors (see Fig. 4).

1. a histogram correlates to the frequency distribution of pixel values for an image region.

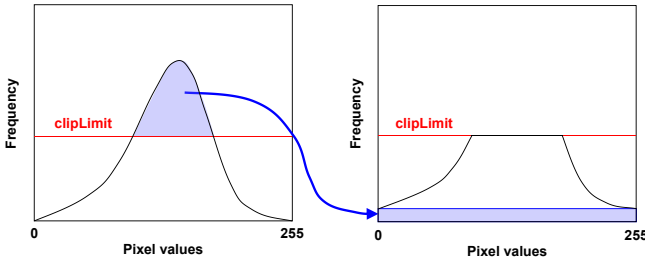


Fig. 3: Clipping

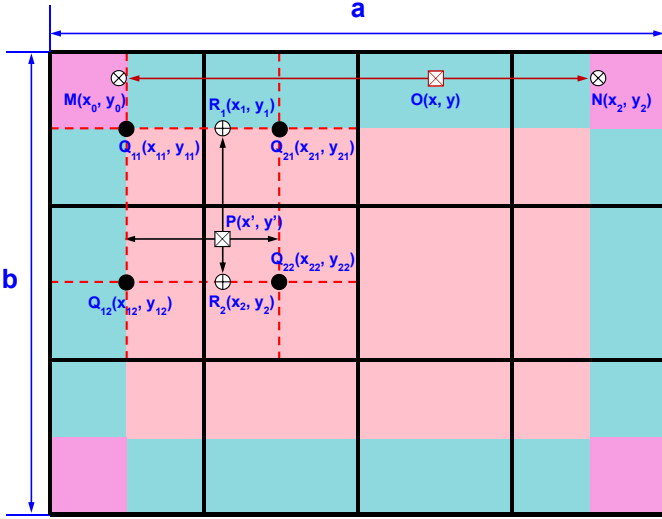


Fig. 4: Transformation of Input Pixels

Each area includes the upper and left borders as well as the outermost border of the image if it is a boundary one. The input pixel values in the rectangle areas shaded purple, sky blue, and pink are transformed by histogram equalization, linear interpolation, and bilinear interpolation, respectively. More specifically, according to [34], pixels in the purple areas and the center pixel of each region are transformed by histogram equalization; each pixel in the sky blue areas is transformed based on two collinear pixels in the two neighboring purple areas by linear interpolation; and pixels in the pink area that lie between two collinear center pixels are transformed by linear interpolation while other pink pixels are transformed by bilinear interpolation based on the four neighboring center pixels. For example, consider the points M , N , Q_{11} , Q_{12} , Q_{21} , Q_{22} , O , R_1 , R_2 , P in different areas of Fig. 4, where the value of the x -coordinate for each pixel point is the input pixel value, and that of the y -coordinate is the output pixel value. The point M in the purple area and the center points Q_{11} , Q_{12} , Q_{21} , and Q_{22} of the four regions in the upper-left of the image are transformed by histogram equalization according to the following transformation function

$$y = h_R(x) = \text{round}\left(\frac{cdf(x) - cdf_{\min}}{cdf_{\max} - cdf_{\min}} \times (L - 1)\right) \quad (2)$$

over all the input pixel values in the image region the point lies in to produce its output pixel value, where cdf_{\min} is the minimum non-zero value of the cumulative distribution

function calculated in the Cumulation phase while cdf_{\max} gives the maximum value.

Note that (2) maps a narrow range of the input pixel values to the full range of the image pixel values. However, this equation may overamplify the small amounts of noises in largely homogeneous image regions [35]. For example, if most pixel values are big numbers, and noises' pixel values are small numbers, the transformation of the noises may fall into the same pixel value such that the noises are overamplified as the frequency of the corresponding pixel values increases. Clipping is thus adopted to equally redistribute the strongly peaked pixel values in the histogram in order to limit the amplification of the noises when the frequency of the pixel values surpasses a prescribed threshold $clipLimit$.

On the other hand, a point O in the sky blue area located at the horizontal line MN , where M and N with pixel value x_0 and x_2 , respectively, are points in the left-upper and right-upper corner purple areas of the image, can be linearly interpolated as follows:

$$y = \frac{x_2 - x}{x_2 - x_0} h_{R_M}(x_0) + \frac{x - x_0}{x_2 - x_0} h_{R_N}(x_2) \quad (3)$$

Besides, point P , an arbitrary point in the pink area, is bilinearly interpolated: its input pixel value x' is transformed to the output pixel value y' based on the input pixel values and output pixel values of the four neighboring center points (Q_{11} , Q_{12} , Q_{21} , and Q_{22}) according to equations (4), (5), and (6). Specifically, (4) and (5) respectively compute the output pixel values of R_1 and R_2 , which are then employed by (6) to generate the output pixel value of P .

$$y_1 = \frac{x_{21} - x_1}{x_{21} - x_{11}} h_{R_{Q_{11}}}(x_{11}) + \frac{x_1 - x_{11}}{x_{21} - x_{11}} h_{R_{Q_{21}}}(x_{21}) \quad (4)$$

$$y_2 = \frac{x_{22} - x_2}{x_{22} - x_{12}} h_{R_{Q_{12}}}(x_{12}) + \frac{x_2 - x_{12}}{x_{22} - x_{12}} h_{R_{Q_{22}}}(x_{22}) \quad (5)$$

$$y' = \frac{y_2 - h_{R_P}(x')}{y_2 - y_1} y_1 + \frac{h_{R_P}(x') - y_1}{y_2 - y_1} y_2 \quad (6)$$

One can see that Transformation makes the pixel values inter-related, enhancing the contrast of the image. Next, the transformed image is resized with a shape (s, s) and then input to Classifier.

3.2.3 Classifier

Classifier estimates the probabilities at which a malware sample is classified to a certain family by employing a CNN algorithm. The classifier employed by our study for the dataset presented in Section 4 is shown in Fig. 5, which contains 12 layers: four convolutional layers, four max-pooling layers, one dropout layer, and three fully connected feed-forward layers, and are detailed in the following paragraph. CNN is adopted here because it has demonstrated promising classification results in many fields, particularly in image processing, which could precisely distinguish different malware families for our purpose.

The classifier in Fig. 5 is constructed with a training dataset that consists of a collection of different types of malware programs. The input is a 2-D vector with a shape of (w, h) , where w and h are respectively the width and height of an image. This vector is first reshaped into a 3-D vector with a shape of $(w, h, 1)$ to meet the shape requirements of the first convolutional layer. The first convolutional layer

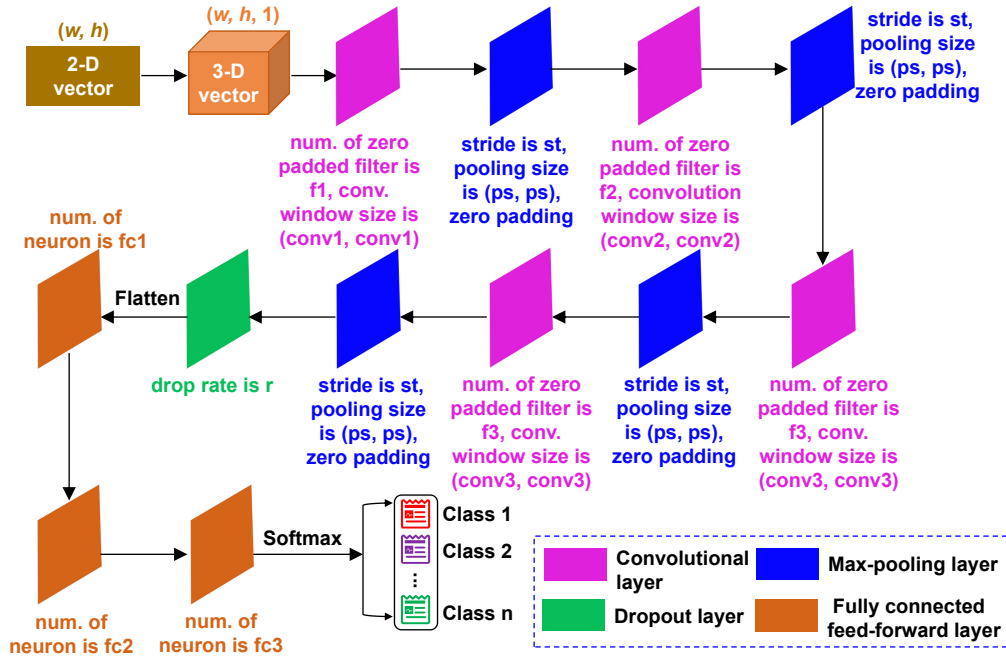


Fig. 5: Network Structure of Classifier

contains f_1 zero-padded filters and a convolution window with a shape of $(conv1, conv1)$. One can get the output of this layer with more channels in-depth, i.e., X_1^C has the shape of (w, h, f_1) . To avoid over-fitting, all convolutional layers would have an L2 regularization penalty with a regularization factor l_2 on the layer's kernel. Following the first convolutional layer is the first max-pooling layer with a stride st , a pooling size (ps, ps) , and zero paddings. All following max-pooling layers have the same settings. The output of the first max-pooling layer is input to the second convolutional layer that contains f_2 zero-padded filters and a convolution window shaped $(conv2, conv2)$. The output from the second convolutional layer is sent to the second max-pooling layer, followed by the third convolutional layer possessing f_3 zero-padded filters and a convolution window shaped $(conv3, conv3)$, and the third max-pooling layer. The output of the third max-pooling layer is processed by the fourth convolutional layer and the fourth max-pooling layer, which are configured similarly to the previous convolutional layer and max-pooling layer. The dropout layer with a drop rate r following the fourth max-pooling layer plays the role of promoting generalization. The output of the dropout layer is flattened and then sent to the first fully-connected feed-forward layer with fc_1 neurons, followed by the second and third fully-connected feed-forward layer with fc_2 and fc_3 neurons, respectively. Note that fc_3 is the number of malware families our dataset has. Also, note that the third fully-connected feed-forward layer contains a softmax activation function that gives the probability of the malware being classified to a certain family, and the calculation is shown in (7).

$$X_{i,j}^C = \frac{\exp(X_{i,j}^C)}{\sum_k \exp(X_{i,k}^C)}. \quad (7)$$

where $X_{i,j}^C$ is the output value of the i th layer that is relevant to the j th malware family. The loss function of the *classifier* is defined in (8), where y_i is the true label of a malware sample, and \hat{y}_i is the predicted label for the malware sample.

$$Loss = - \sum_{i=1}^{f_3} y_i \log \hat{y}_i \quad (8)$$

To precisely distinguish different types of malware in the dataset, *Loss* should be minimized about the weights and parameters of the *classifier*. Minimizing *Loss* would improve the predicted probability of malware that belongs to its corresponding family. When employing the *classifier* to test a malware sample, the input is a malware image and the output is the malware family the image (malware) belongs to.

4 EVALUATION

The metrics to measure the performance of VisMal include *accuracy*, *efficiency*, and *visualization*. Let $C_{i,j}$ be the number of malware samples in family i that are classified to family j by Classifier, where $i, j \in \{1, 2, \dots, N\}$ and N is the total number of malware families. Then one can utilize TP, FN, FP, and TN, the four common machine learning parameters to define the performance metrics of VisMal. More specifically, for a malware family i , TP_i provides the number of correctly predicted samples belonging to the family i , represented by $TP_i = C_{i,i}$; TN_i is the number of correctly predicted samples belonging to other families, represented by $TN_i = \sum_{j=1, j \neq i}^N C_{j,j}$; FN_i is the number of misclassified samples that

belong to family i , represented by $FN_i = \sum_{j=1}^N C_{i,j} - C_{i,i}$ and FP_i is the number of samples misclassified into family

i , represented by $FP_i = \sum_{j=1}^N C_{j,i} - C_{i,i}$. Then, the metrics to examine the performance of Classifier can be formally denoted as:

- 1) The *accuracy* is the ratio of correctly predicted malware samples over all malware samples:

$$accuracy = \frac{TP_i + TN_i}{TP_i + FN_i + FP_i + TN_i}. \quad (9)$$

- 2) The *precision* for a malware family i is the ratio of correctly classified samples over the total samples classified into this family:

$$precision = \frac{TP_i}{TP_i + FP_i}. \quad (10)$$

- 3) The *recall* for a malware family is the ratio of correctly classified samples over the total samples belonging to this family:

$$recall = \frac{TP_i}{TP_i + FN_i}. \quad (11)$$

- 4) The *F1 score* for a malware family i is the balanced average of precision and recall:

$$F1\ score = \frac{2 * (recall * precision)}{recall + precision}. \quad (12)$$

We also examine the efficiency of our VisMal framework. As VisMal is a time-sensitive system, its efficiency, denoted by *MPE*, can be measured by the CPU processing time per malware sample that counts only feature extraction and classification. Let *cputime* be the total clock ticks used to process *num_files* malware samples. We have

$$MPE = \frac{cputime}{num_files}. \quad (13)$$

Besides accuracy and efficiency, we also employ visualization to validate the performance of VisMal, providing security engineers with a convenient way to further analyze malware samples.

4.1 Experiment Setup

Equipment and Dataset. The PC employed by VisMal is equipped with 12 processors, 6 kernels, and an installed RAM with a 32.0GB available memory running the 64-bit Windows 10 operating system. Each processor is configured with Intel(R) Core(TM) i7-8750 CPU @2.20GHz, 2201Mhz. The versions of Keras, Tensorflow, Pillow, and OpenCV to develop our framework are 2.2.3, 2.4.0, 6.2.1, and 4.5.1.48, respectively. Additionally, we adopt the Maling dataset released by the Vision Researchcomprises Lab at the University of California, Santa Barbara, as training and test data [36]. This dataset comprises 9339 malware samples in total, which belongs to 25 malware families with a varying number of malware files per family, as detailed in Table 2.

Parameters. In order to identify a proper structure of Classifier, we attempted the number of layers from 1 to 20. It turned out that a structure with 12 layers is the most effective one considering the trade-off between accuracy and efficiency when Classifier without Transformation is employed to distinguish malware images. More specifically,

TABLE 2: Maling Dataset

number	Family	num_files
1.	Adialer.C	122
2.	Agent!FYI	116
3.	Allapple.A	2949
4.	Allapple.L	1591
5.	Alueron.gen!J	198
6.	Autorun.K	106
7.	C2Lop.gen!g	200
8.	C2Lop.P	146
9.	Dialplatform.B	177
10.	Dontovo.A	162
11.	Fakerean	381
12.	Instantaccess	431
13.	Lolyda.AA 1	213
14.	Lolyda.AA 2	184
15.	Lolyda.AA 3	123
16.	Lolyda.AT	159
17.	Malex.gen!J	136
18.	Obfuscator.AD	142
19.	Rbot!gen	158
20.	Skintrim.N	80
21.	Swizzot.gen!E	128
22.	Swizzot.gen!I	132
23.	VB.AT	408
24.	Wintrim.BX	97
25.	Yuner.A	800

TABLE 3: Model Parameters for Classifier

Parameters	Implications	Values
w	width of image	64
h	height of image	64
$f1$	num of filters	64
$conv1$	kernel size	5
$l2$	kernel regularizer	0.01
st	stride	1
ps	pooling size	2
$f2$	num of filters	128
$conv2$	kernel size	5
$f3$	num of filters	256
$conv3$	kernel size	2
r	drop rate	0.5
$fc1$	num of neurons	256
$fc2$	num of neurons	128
$fc3$	num of taxonomies	25

the constructed classifier includes 4 convolutional layers, 4 max-pooling layers, 1 dropout layer, and 3 fully connected feed-forward layers. The details of the model parameters are presented in Table 3.

Once the structure of Classifier is fixed, we next determine the values of the following parameters defined in Section 3.2.2, which are used by the Transformation phase, in order to attain a better performance: a and b , the numbers of pieces split up respectively for the width and height of a malware image during the Transformation phase; $clipLimit$, the upper bound of the frequency of a pixel value adopted by the Clipping phase; and s , the number of pixels in the width and height of the transformed malware image to be inputted to Classifier at the end of Transformation. In our experiments, $clipLimit$ is empirically set to be 4 according to [34], and the shape s of a transformed image is set to be 64 (the least image width) concerning the trade-off between accuracy and efficiency since a too small value of s incurs a loss of image information while a too big value is bad for the fast processing of Classifier.

The determination of a and b is more complicated. Since different programs were developed for different purposes and thus have different sets of instructions to support their functionality, we consider the distribution of the instruction length to determine the value of a . In [37], Ibrahim *et al.* counted instruction length distributions for different types of programs, whose values were used to get the statistical information shown in Table 4. One can see that, for all types of programs, 64-bit executables and DLLs have the largest weighted average instruction length, i.e., 3.1 bytes; thus we round up the length to 4 bytes to accommodate an entire instruction in most cases. Correspondingly, we fix the width of an image region for all malware images, which should be a multiple of 4 intuitively. As a result, the value of a varies for different malware images due to various image widths. Next we need to figure out the value of b . For simplicity, we choose a fixed b determined by the average height of all malware samples belonging to the same family even though they may own different file sizes whose discrepancies are huge. Nevertheless, a big value of b (too many pieces in height) separates similar instruction sequences into different image regions, while a small value decreases the effectiveness of Transformation to enhance the local contrast at each image region. Based on the above considerations, we tested the classification accuracy of all images in our dataset and attempted values of 8, 16, 32, 48, and 64 for the width of an image region, and values of 20 to 24 for the value of b , and selected the value of 32 and 23 respectively for the width of an image region and b . The detailed settings of a and b are listed in Table 5.

TABLE 4: Weighted Average Instruction Length for Each Application Category

Application Category	Weighted Average Instruction Length
Web Browsers	3.0
Graphics Applications	2.3
OS related components	2.7
General Purpose Applications	2.9
Software Development Tools	2.5
32-bit Executables and DLLs	2.4
64-bit Executables and DLLs	3.1
sum	2.5

TABLE 5: The Distribution of Malware Sample File Sizes

File Size	num_of_files	Width	a	Height	b
< 10KB	0	32	0	(0,320]	0
10KB-30KB	701	64	2	(156,468]	23
30KB-60KB	1901	128	4	(234,468]	23
60KB-100KB	3209	256	8	(234, 390]	23
100KB-200KB	1116	384	12	(260,520]	23
200KB-500KB	1071	512	16	(390, 976]	23
500KB-1000KB	1324	768	24	(651,1302]	23
1000KB ≤	17	1024	32	(976, ∞)	23

4.2 Evaluation Results

4.2.1 Accuracy

We first evaluate the accuracy of VisMal over the Maling dataset and then compare VisMal with its variant, i.e., the

TABLE 6: Classification Report

Malware Family	Precision	Recall	F1 Score	accuracy
Adialer.C	99.2	100	99.6	100
Agent.FYI	97.8	100	98.8	100
Allaple.A	99.6	99.9	99.7	99.9
Allaple.L	99.9	99.9	100	99.9
Alueron.gen!J	99.5	98.0	98.7	98.0
Autorun.K	9.4	9.4	9.4	9.4
C2LOP.gen!g	84.5	80.5	78.3	80.5
C2LOP.P	76.1	76.8	75.2	76.7
Dialplatform.B	99.5	100	99.7	100
Dontovo.A	99.4	100	99.7	100
Fakerean	99.2	98.3	98.8	98.4
Instantaccess	99.8	100	99.9	100
Lolyda.AA1	97.9	96.7	97.1	96.7
Lolyda.AA2	97.1	97.8	97.2	97.8
Lolyda.AA3	99.2	97.6	98.3	97.6
Lolyda.AT	98.2	98.2	98.2	98.1
Malex.gen!J	97.3	97.8	97.2	97.8
Obfuscator.AD	100	100	100	100
Rbot!gen	94.4	94.5	94.0	94.3
Skintrim.N	87.8	90.0	88.8	90.0
Swizzor.gen!E	52.8	47.6	46.1	47.7
Swizzor.gen!I	51.1	43.3	37.0	43.2
VB.AT	99.1	97.9	98.5	97.8
Wintrim.BX	99.1	97.9	98.5	97.9
Yuner.A	89.5	100	94.6	100
weighted avg	95.3	96.0	95.2	96.0

version of VisMal without the Transformation phase, and a few other methods using different techniques. We conducted 10-fold stratified cross-validation to examine the accuracy of VisMal. This approach ensures an approximately equal proportion of each family present at each fold. Among the 10 folds, 9 is used for the training procedure and the rest is reserved for the test procedure. We repeated this process 10 times, with each fold used exactly once as the test fold, to ensure that all malware samples are used for testing purposes to check VisMal’s generalization ability. Finally, the average accuracy, precision, recall, and F1 score are computed for all malware families and the results are reported in Table 6.

One can see from Table 6 that the average accuracy, precision, recall, and F1 score of VisMal are 96.0%, 95.3%, 96.0% and 95.2%, respectively. Specifically, among the 25 malware families, most of them are characterized correctly, with an accuracy close to 98% or above. Note that some of the malware samples, including Yuner.A, VB.AT, Malex.gen!J, Autorun.K, and Rbot!gen in our dataset, possess similar structures and patterns, and are packed by the UPX packer; thus it is difficult for VisMal to separate them. But VisMal still achieves a promising result for all of them except Autorun.K. Specifically, VisMal classifies Yuner.A with a recall of 100%, VB.AT of 97.9%, Malex.gen!J of 97.8%, and Rbot!gen of 94.5%. Through a manual analysis, we found that the converted images of Autorun.K are extremely similar to those of Yuner.A. They are hard to be distinguished by human eyes as demonstrated by Fig. 6. As a result, all misclassified Autorun.K malware samples are classified into Yuner.A, as illustrated by the confusion matrix in Table 7 that shows the specific classification results. It should also be noted that the code sections of Allaple.A and Allaple.L are encrypted at several layers using random keys; but they

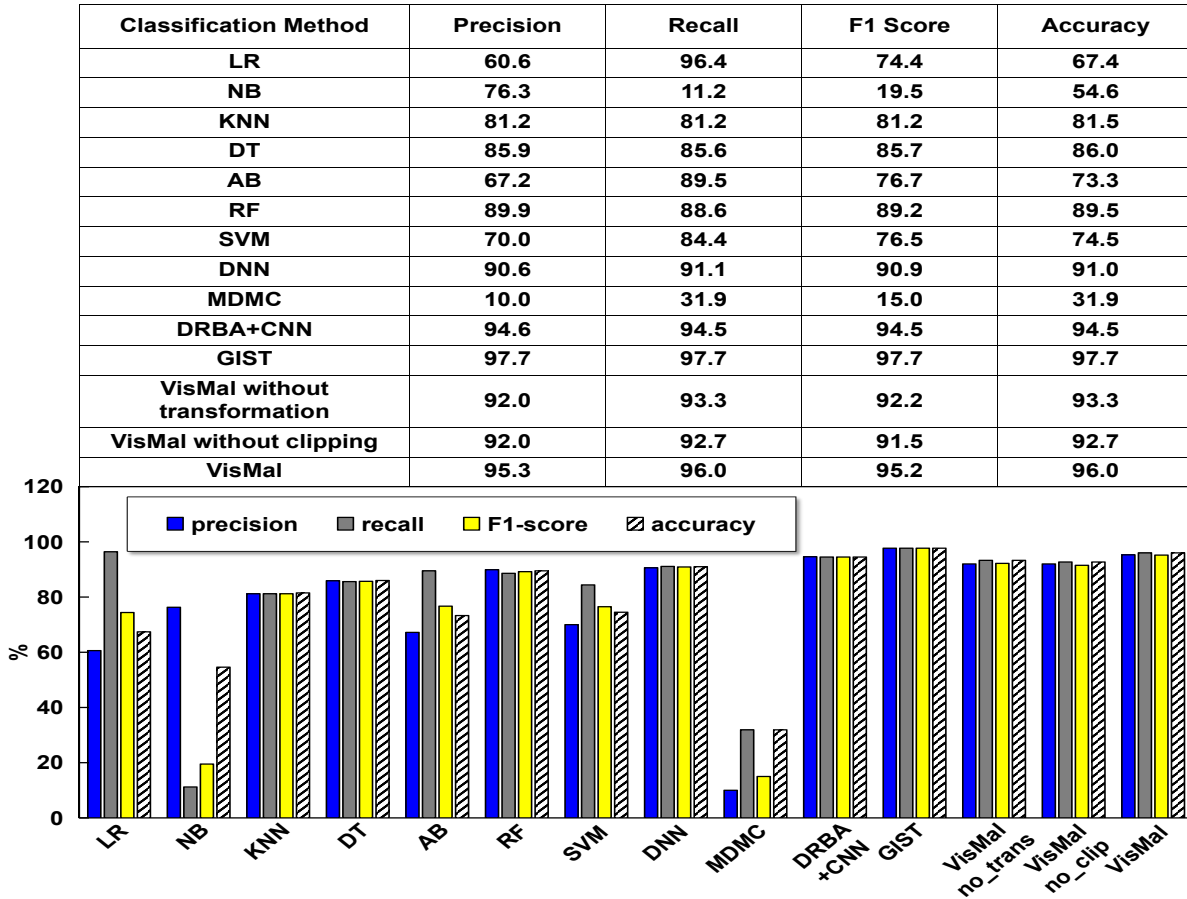


Fig. 8: Accuracy of the Classification Methods

accuracy of 96.0%. To be specific, among the 7 common machine learning-based classification techniques and the deep learning-based approach presented in [38], the deep learning-based method demonstrates the best performance with an accuracy of 91%, and LR achieves a very high recall at a moderate accuracy because the classifier categorizes a lot of malware samples from other families to the rest of them. The CNN-based framework proposed in [39], namely DRBA+CNN, employs a BAT algorithm that can properly balance the number of samples in different malware families, achieving an accuracy of 94.5%. Besides, we reimplemented two malware image-based frameworks, namely GIST and MDMC that were respectively proposed in [29] and [31], where GIST utilizes the Gabor filters to extract statistical features for each malware gray image and carefully selects 320 features as the input to the k -nearest neighbor algorithm for final classification, while MDMC converts malware binaries into Markov probability matrixes by counting the frequency of two neighboring bytes and then employs a deep convolutional neural network to categorize different Markov probability matrixes. One can see that although GIST performs slightly better than VisMal in accuracy, its efficiency is far slower (described later). On other other hand, VisMal significantly outperforms MDMC in malware classification.

TABLE 8: Efficiency of the Classification Methods

	Extraction Time	Classification Time	Total Time
Nataraj <i>et al.</i> [29]	32.7 ms	2.1 ms	34.8 ms
Cui <i>et al.</i> [39]	-	-	20 ms
Naeem <i>et al.</i> [40]	-	4.27 s	-
Yuan <i>et al.</i> [31]	144.3 ms	191.5 ms	335.8 ms
Vasan <i>et al.</i> [41]	-	-	1.18 s
Verma <i>et al.</i> [30]	37 ms	10 ms	47 ms
VisMal	0.3 ms	3.7 ms	4.0 ms

4.2.2 Efficiency

Since malware classification is a time-sensitive component in any anti-virus product, and a small delay could miss the best opportunity to discover malware processes, the procedure for distinguishing malware samples should take short time. We measured the CPU time of our dataset passing through VisMal during the test procedure and calculated the average MPE per malware sample. To consider a practical setting for evaluating VisMal, we did not deploy it on servers or call GPUs. The efficiency evaluation results are reported in Table 8. One can see that VisMal incurs 0.3 ms on feature extraction and 3.7 ms on classification, efficiently providing information to anti-virus products for further operations. Besides, we compared VisMal with the techniques presented by the latest research ([29] in 2011, [39] in 2018, [40] in 2019, [31] in 2020, [41] in 2020, and [30] in 2020) that mainly pay attention to efficiency on malware

classification over the same dataset. From Table 8 we notice that VisMal takes the least extraction time and total time, and the second least classification time. Specifically, in terms of the time taken to extract features, VisMal is 108 times faster than the method proposed by Nataraj *et al.*, and 122.33 times faster than the method presented by Verma *et al.* Additionally, the classification time incurred by VisMal is reduced by 1153.05 times and 1.70 times compared with the approaches in Naeem *et al.* and Verna *et al.*, respectively. Besides the extraction time and classification time, a significant decrease in total time (4 times) is reported for VisMal, when compared to Cui *et al.*, the second-fastest method reported in Table 8.

4.2.3 Visualization

Since malware classification is an important component integrated into all anti-virus tools, its precision plays an essential role in making these tools effective. To analyze the performance of VisMal, this section presents the visualization results in which malware samples are converted into images and then processed by the contrast-limited adaptive histogram equalization algorithm. Visualization provides useful information for manual analysis to ascertain whether the categorized malware samples are similar, which can help to confirm the performance of VisMal from a different angle. As VisMal converts malware samples into images, it naturally offers security engineers a convenient way to analyze malware samples and look for reasons when they are misclassified, based on which security engineers can integrate new techniques to improve the performance of their anti-virus products. Fig. 9 demonstrates the texture similarity among malware samples belonging to the same family and dissimilarity from those belonging to different families. As shown in 9a-9b, 9c-9d, 9e-9f, 9g-9h, 9i-9j, 9k-9l, one can see that each pair is almost indistinguishable in terms of their texture information since, in the same family, the samples share certain common instruction sequences, and correspondingly their malware images tend to be similar in certain regions. Conversely, malware samples belonging to different families, which are developed for different purposes, make use of a dissimilar set of instruction sequences and thus have a huge difference in pixels' distribution, see Figs. 9a and 9g as an example.

5 CONCLUSION AND FUTURE RESEARCH

In this paper, we propose a novel, efficient, and effective simple malware categorization framework titled VisMal, which can discover the underlying byte code similarity for malware samples that belong to a particular family. On one hand, VisMal alleviates the difficulty of security engineers to study the complicated structures of different malware samples based on static analysis, and in the meantime significantly improves the classifying efficiency from dynamic analysis. On the other hand, VisMal focuses on texture representation by converting malware samples into images, effectively subverting the traditional ways of understanding binary information.

Note that VisMal pays attention to disclose the encoding art in byte codes and makes use of encoding to interpret the similarity of malware samples belonging to the same

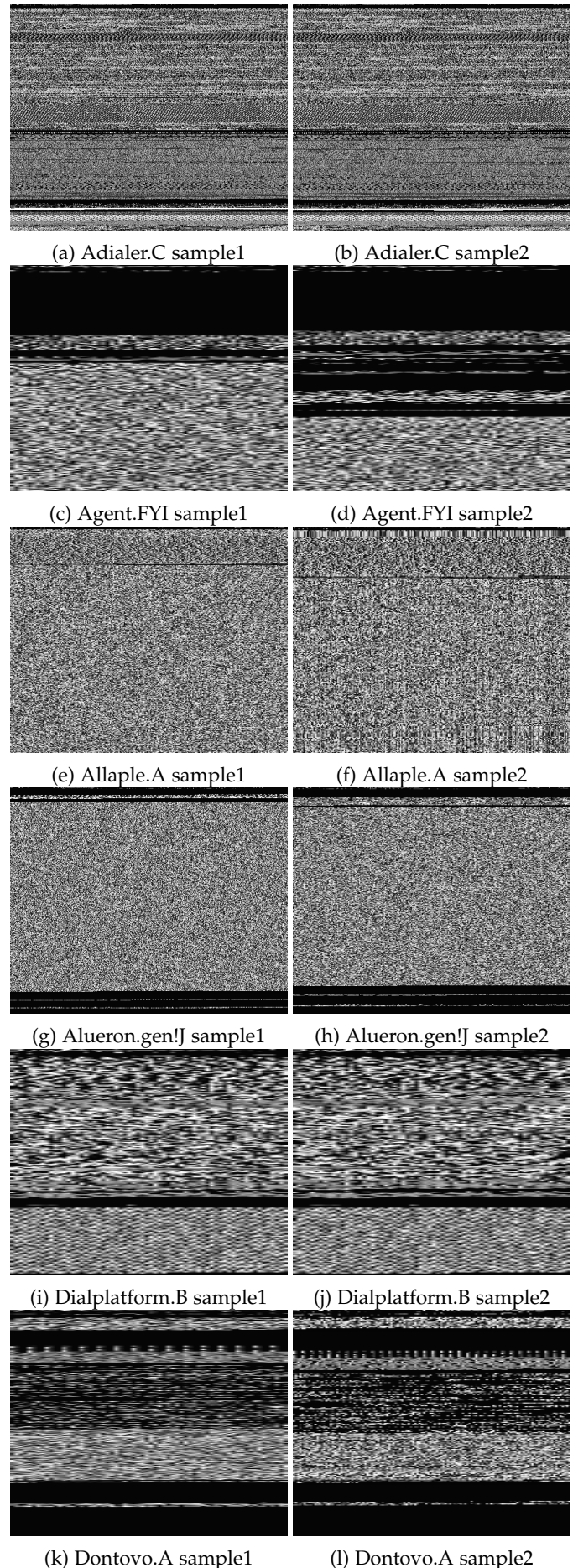


Fig. 9: Visual Similarity Example 3

family and dissimilarity between different malware families. To improve the accuracy of classification, VisMal exploits a contrast-limited adaptive histogram equalization algorithm to increase the local contrast of each region for a malware image, and effectively transfers from looking for similar codes to similar image regions. Moreover, VisMal provides a simple and convenient way for security engineers to validate the performance of classification and to further analyze the factors confusing Classifier such that its performance can be improved by adding new techniques into anti-virus products.

Our future research will be committed to finding out the close relationship between the critical information of malware images learned by neural networks and the byte-code sequences, which may contribute to the extraction of signatures on behalf of a malware family. Such signatures can be managed via blockchain technologies [42]–[44] to facilitate malware detection by a broader audience. We are also interested in the discovery of vulnerabilities in programs by making use of visualization techniques, which could provide new insights to help developers improve their codes for better classification performance. Besides, we will further strengthen our framework to distinguish malware and benignware.

REFERENCES

- [1] A. Pekta and T. Acarman, "Classification of malware families based on runtime behaviors," *Journal of Information Security and Applications*, vol. 37, pp. 91–100, 2017. [Online]. Available: <https://www.sciencedirect.com/science/article/pii/S2214212617301643>
- [2] C. C. San, M. M. S. Thwin, and N. L. Htun, "Malicious software family classification using machine learning multi-class classifiers," in *Computational Science and Technology*, R. Alfred, Y. Lim, A. A. A. Ibrahim, and P. Anthony, Eds. Singapore: Springer Singapore, 2019, pp. 423–433.
- [3] F. Zhong, X. Cheng, D. Yu, B. Gong, S. Song, and J. Yu, "Malfox: Camouflaged adversarial malwareexample generation based on conv-gans againstblack-box detectors," <https://arxiv.org/pdf/2011.01509.pdf>, 2020.
- [4] A. Moser, C. Kruegel, and E. Kirda, "Limits of static analysis for malware detection," in *Twenty-Third Annual Computer Security Applications Conference (ACSAC 2007)*, Miami Beach, FL, USA, 2007, pp. 421–430.
- [5] M. Y. Wong and D. Lie, "Intellidroid: A targeted input generator for the dynamic analysis of android malware," in *Network and Distributed System Security Symposium*, 2015, pp. 1–15.
- [6] A. Calleja, J. Tapiador, and J. Caballero, "The malsource dataset: Quantifying complexity and code reuse in malware development," *IEEE Transactions on Information Forensics and Security*, vol. 14, no. 12, pp. 3175–3190, 2019.
- [7] D. Korczynski and H. Yin, "Capturing malware propagations with code injections and code-reuse attacks," in *Proceedings of the 2017 ACM SIGSAC Conference on Computer and Communications Security (CCS'17)*, October 2017, pp. 1691–1708.
- [8] N. Marastoni, A. Continella, D. Quarta, S. Zanero, and M. D. Preda, "Groupdroid: Automatically grouping mobile malware by extracting code similarities," in *Proceedings of the 7th Software Security, Protection, and Reverse Engineering/Software Security and Protection Workshop (SSPREW-7)*, no. 1, December 2017, pp. 1–12.
- [9] —, "Andro-profiler: anti-malware system based on behavior profiling of mobile malware," in *Companion: Proceedings of the 23rd International Conference on World Wide Web*, April 2014, pp. 737–738.
- [10] J. Jiang, S. Li, M. Yu, G. Li, C. Liu, K. Chen, H. Liu, and W. Huang, "Android malware family classification based on sensitive opcode sequence," in *2019 IEEE Symposium on Computers and Communications (ISCC)*, 2019, pp. 1–7.
- [11] F. Fasano, F. Martinelli, F. Mercaldo, and A. Santone, "Cascade learning for mobile malware families detection through quality and android metrics," in *2019 International Joint Conference on Neural Networks (IJCNN)*, 2019, pp. 1–10.
- [12] W. Blanc, L. G. Hashem, K. O. Elish, and M. J. Hussain Almohri, "Identifying android malware families using android-oriented metrics," in *2019 IEEE International Conference on Big Data (Big Data)*, 2019, pp. 4708–4713.
- [13] B. Jung, T. Kim, and E. G. Im, "Malware classification using byte sequence information," in *Proceedings of the 2018 Conference on Research in Adaptive and Convergent Systems (RACS'18)*, 2018, pp. 143–148.
- [14] J. Saxe and K. Berlin, "Deep neural network based malware detection using two dimensional binary program features," in *2015 10th International Conference on Malicious and Unwanted Software (MALWARE)*, 2015, pp. 11–20.
- [15] A. Davis and M. Wolff, "Deep learning on disassembly data," <https://paper.seebug.org/papers/Security20Conf/Blackhat/2015/us-15-Davis-Deep-Learning-On-Disassembly.pdf>, 2015.
- [16] J. Kinable and O. Kostakis, "Malware classification based on call graph clustering," *Journal in Computer Virology*, vol. 7, pp. 233–245, 2011. [Online]. Available: <https://link.springer.com/article/10.1007/s11416-011-0151-yciteas>
- [17] O. Mirzaei, G. S. Tangil, J. M. de Fuentes, J. Tapiador, and G. Stringhini, "Andrensemble:leveraging api ensembles to characterize android malware families," in *Proceedings of the 2019 ACM Asia Conference on Computer and Communications Security (Asia CCS'19)*, 2019, pp. 307–314.
- [18] M. Zhang, Y. Duan, H. Yin, and Z. Zhao, "Semantics-aware android malware classification using weighted contextual api dependency graphs," in *Proceedings of the 2014 ACM SIGSAC Conference on Computer and Communications Security (CCS'14)*, November 2014, pp. 1105–1116.
- [19] K. Sethi, R. Kumar, L. Sethi, P. Bera, and P. K. Patra, "A novel machine learning based malware detection and classification framework," in *2019 International Conference on Cyber Security and Protection of Digital Services (Cyber Security)*, 2019, pp. 1–4.
- [20] A. Martin, V. Rodriguez-Fernandez, and D. Camacho, "Candyman: Classifying android malware families by modeling dynamic traces with markov chains," *Engineering Applications of Artificial Intelligence*, vol. 74, pp. 121–133, 2018. [Online]. Available: <https://www.sciencedirect.com/science/article/abs/pii/S0952197618301374>
- [21] B. Anderson, D. Quist, J. Neil, C. Storlie, and T. Lane, "Graph-based malware detection using dynamic analysis," *Journal in Computer Virology*, vol. 7, pp. 247–258, 2011. [Online]. Available: <https://link.springer.com/article/10.1007/s11416-011-0152-xciteas>
- [22] G. E. Dahl, J. W. Stokes, L. Deng, and D. Yu, "Large-scale malware classification using random projections and neural networks," in *2013 IEEE International Conference on Acoustics, Speech and Signal Processing*, 2013, pp. 3422–3426.
- [23] S. Tobiyama, Y. Yamaguchi, H. Shimada, T. Ikuse, and T. Yagi, "Malware detection with deep neural network using process behavior," in *2016 IEEE 40th Annual Computer Software and Applications Conference (COMPSAC)*, vol. 2, 2016, pp. 577–582.
- [24] Z. Zhang, P. Qi, and W. Wang, "Dynamic malware analysis with feature engineering and feature learning," in *Proceedings of the AAAI Conference on Artificial Intelligence*, vol. 34, no. 01, 2020, pp. 1210–1217.
- [25] D. Vij, V. Balachandran, T. Thomas, and R. Surendran, "Gramac: A graph based android malware classification mechanism," in *Proceedings of the Tenth ACM Conference on Data and Application Security and Privacy (CODASPY'20)*, 2020, pp. 156–158.
- [26] Y. Park, D. Reeves, V. Mulukutla, and B. Sundaravel, "Fast malware classification by automated behavioral graph matching," in *Proceedings of the Sixth Annual Workshop on Cyber Security and Information Intelligence Research*, 2010, pp. 1–4.
- [27] S. Hsiao, Y. S. Sun, and M. C. Chen, "Behavior grouping of android malware family," in *2016 IEEE International Conference on Communications (ICC)*, 2016, pp. 1–6.
- [28] L. Nataraj, V. Yegneswaran, P. Porras, and J. Zhang, "A comparative assessment of malware classification using binary texture analysis and dynamic analysis," in *Proceedings of the 4th ACM workshop on Security and artificial intelligence (AISec'11)*, October 2011, pp. 21–30.
- [29] L. Nataraj, S. Karthikeyan, G. Jacob, and B. S. Manjunath, "Malware images:visualization and automatic classification," in *Proceedings of the 8th International Symposium on Visualization for Cyber Security (VizSec'11)*, vol. 4, July 2011, pp. 1–7.

- [30] V. Verma, S. K. Muttoo, and V. Singh, "Multiclass malware classification via first- and second-order texture statistics," *Computers & Security*, vol. 97, p. 101895, 2020. [Online]. Available: <https://www.sciencedirect.com/science/article/pii/S0167404820301681>
- [31] B. Yuan, J. Wang, D. Liu, W. Guo, P. Wu, and X. Bao, "Byte-level malware classification based on markov images and deep learning," *Computers & Security*, vol. 92, p. 101740, 2020. [Online]. Available: <https://www.sciencedirect.com/science/article/pii/S0167404820300262>
- [32] D. Hargreaves, "Stratified k-fold: What it is & how to use it," <https://towardsdatascience.com/stratified-k-fold-what-it-is-how-to-use-it-cf3d107d3ea2>, 2021.
- [33] R. Dorothy, R. Joany, R. J. Rathish, S. S. Prabha, and S. rajendran, "Image enhancement by histogram equalization," *Int. J. Nano. Corr. Sci. Engg.*, vol. 2, no. 4, pp. 21–30, 2015.
- [34] "Adaptive histogram equalization," <https://en.wikipedia.org/wiki/Adaptivehistogramequalizationcite-note-clahe87-3>, 2021.
- [35] K. Zuiderveld, "Contrast limited adaptive histogram equalization," <http://cas.xav.free.fr/Graphics%20Gems%204%20-%20Paul%20S.%20Heckbert.pdf>, 1993.
- [36] "Signal processing for malware analysis," <https://vision.ece.ucsb.edu/research/signal-processing-malware-analysis>, 2021.
- [37] A. H. Ibrahim, M. B. Abdelhalim, H. Hussein, and A. Fahmy, "An analysis of x86-64 instruction set for optimization of system softwares," *International Journal of Advanced Computer Science*, vol. 1, no. 4, pp. 152–162, 2011.
- [38] R. Vinayakumar, M. Alazab, K. P. Soman, P. Poornachandran, and S. Venkatraman, "Robust intelligent malware detection using deep learning," *IEEE Access*, vol. 7, pp. 46717–46738, 2019.
- [39] Z. Cui, F. Xue, X. Cai, Y. Cao, G. Wang, and J. Chen, "Detection of malicious code variants based on deep learning," *IEEE Transactions on Industrial Informatics*, vol. 14, no. 7, pp. 3187–3196, 2018.
- [40] H. Naeem, B. Guo, M. R. Naeem, F. Ullah, H. Aldabbas, and M. S. Javed, "Identification of malicious code variants based on image visualization," *Computers & Electrical Engineering*, vol. 76, pp. 225–237, 2019. [Online]. Available: <https://www.sciencedirect.com/science/article/pii/S004579061733776X>
- [41] D. Vasan, M. Alazab, S. Wassan, B. Safaei, and Q. Zheng, "Image-based malware classification using ensemble of cnn architectures (imcec)," *Computers & Security*, vol. 92, p. 101748, 2020. [Online]. Available: <https://www.sciencedirect.com/science/article/pii/S016740482030033X>
- [42] M. Xu, C. Liu, Y. Zou, F. Zhao, J. Yu, and X. Cheng, "wchain: A fast fault-tolerant blockchain protocol for multihop wireless networks," *IEEE Transactions on Wireless Communication*, 2021. [Online]. Available: <https://arxiv.org/abs/2102.01333>
- [43] M. Xu, F. Zhao, Y. Zou, C. Liu, X. Cheng, and F. Dressler. Blown: A blockchain protocol for single-hop wireless networks under adversarial sinr. [Online]. Available: <https://arxiv.org/abs/2103.08361>
- [44] M. Xu, S. Liu, D. Yu, X. Cheng, S. Guo, and J. Yu. Cloudchain: A cloud blockchain using shared memory consensus and rdma. [Online]. Available: <https://arxiv.org/abs/2106.04122>